Excitons in Bilayer MoS_2 Displaying a Colossal Electric Field Splitting and Tunable Magnetic Response

Etienne Lorchat,[1] Malte Selig,[2] Florian Katsch,[2] Kentaro Yumigeta,[3] Sefaattin Tongay,[3] Andreas Knorr,[2] Christian Schneider,[1,4] and Sven Höfling[1]

[1]*Technische Physik, Wilhelm-Conrad-Röntgen-Research Center for Complex Material Systems, Universität Würzburg, Am Hubland, D-97074 Würzburg, Germany*

[2]*Institut für Theoretische Physik Nichtlineare Optik und Quantenelektronik, Technische Universität Berlin, D-10623 Berlin, Germany*

[3]*School for Engineering of Matter, Transport, and Energy, Arizona State University, Tempe, Arizona 85287, USA*

[4]*Institute of Physics, University of Oldenburg, 26129 Oldenburg, Germany*

(Received 28 April 2020; revised 29 September 2020; accepted 16 December 2020; published 20 January 2021)

van der Waals heterostructures composed of transition metal dichalcogenide monolayers (TMDCs) are characterized by their truly rich excitonic properties which are determined by their structural, geometric, and electronic properties: In contrast to pure monolayers, electrons and holes can be hosted in different materials, resulting in highly tunable dipolar many-particle complexes. However, for genuine spatially indirect excitons, the dipolar nature is usually accompanied by a notable quenching of the exciton oscillator strength. Via electric and magnetic field dependent measurements, we demonstrate that a slightly biased pristine bilayer MoS_2 hosts strongly dipolar excitons, which preserve a strong oscillator strength. We scrutinize their giant dipole moment, and shed further light on their orbital and valley physics via bias-dependent magnetic field measurements.

DOI: 10.1103/PhysRevLett.126.037401

Introduction.—The interest in excitons hosted in atomically thin materials was initially sparked by their giant oscillator strength and large binding energies, resulting from the canonical interplay of reduced dielectric screening and confinement of charge carriers in an atomically thin sheet [1]. The spectacular finding of extreme optical activity triggered a plethora of experiments, analyzing their chirality [2], their magnetic behavior [3–7], interactions yielding higher order multiparticle complexes [8,9] and finally driving the field of opto-electronic applications [10]. In the latter, in particular the coupling to confined microcavity modes became a field of particular interest, giving rise to pronounced polaritonic phenomena up to ambient conditions [11–13]. More recently, the sheet nature of TMDCs, which allows for almost arbitrary stacking and alignment of multiple monolayers, was harnessed to compose more complex electronic structures. One recurrent scheme in devices based on such van der Waals heterostructures is charge transfer phenomena, which yield the formation of dipolar excitons with electrons and holes confined in different layers. Such interlayer excitons have been studied in van der Waals heterostructures [14], as well as homobilayers $MoSe_2$ [15], MoS_2 [16], and $MoTe_2$ [17]. While such excitons do have appealing properties, including enhanced nonlinearities borrowed from their dipolar character, the giant oscillator strength, which initially sparked the success of TMDC excitons, is strongly compromised by the reduced spatial overlap of electrons and holes in separate layers. However, recently it was suggested that the hybridization of hole states in a pristine bilayer of MoS_2 enables the formation of dipolar excitons, which combine a permanent dipole moment with a giant oscillator strength [18] and aspects have been observed experimentally [19]. Here, we give evidence for this new species of TMDC exciton: Their dipolar character is clearly evidenced in field-dependent absorption measurements, which reveal a giant electric field splitting while maintaining a substantial optical absorption maintaining a substantial optical absorption. We further scrutinize the orbital and valley composition by assessing the excitonic g factor in the presence of a static electric field, and develop a consistent microscopic theory describing our main findings.

Experimental results.—In order to characterize interlayer excitons with strong dipole moment in pristine MoS_2 TMDC bilayers, we fabricate a van der Waals heterostructure composed of few layer graphene (FLG), an approx. 13 nm thick layer of hexagonal boron nitride (BN), a pristine bilayer MoS_2, another 13 nm thick BN and FLG [Fig. 1(a)]. Both FLG are electrically contacted to achieve a top and backgate which allows us to apply an out of plane electric field (see the methods section). A microscope image of the fully assembled device is shown in Fig. 1(b).

The excitonic optical response of bilayer MoS_2 is composed by the so-called A- and B-exciton transitions at the K and K' point, respectively. As opposed to a monolayer, charge transfer processes further allow for the emergence of spatially indirect excitonic complexes in

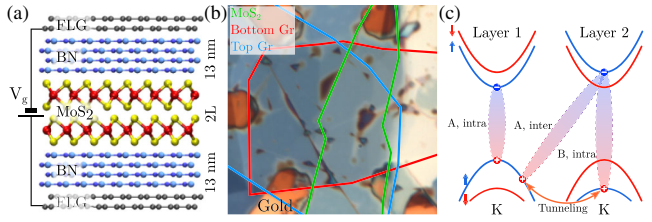

FIG. 1. (a) Sketch of the device, composed of a few layer graphene, boron nitrite, bilayer MoS_2,boron nitrite, few layer graphene sandwhich. (b) Optical micrograph of the sample. (c) Sketch of the exciton states relevant for the optical response in bilayer MoS_2 at the K point. At the K' point (not shown), the spin bands, which are indicated by the color of the respective bands, are reversed.

bilayers, which enriches the optical response. As schematically captured in Fig. 1(c) and anticipated in Refs. [18], [19], a hybrid resonance evolves by hybridizing an A-type interlayer transition with a B-type intralayer resonance. Such a hybrid transition consequently admixes the dipolar properties of interlayer excitons with the strong oscillator strength of TMDC intralayer resonances.

We first probe the optical response of our device via white light reflection spectroscopy at cryogenic temperatures (4 K), and plot the differential reflectivity $\Delta R/R$ normalized with respect to a reference spectrum recorded next to the structure. At zero gate voltage, we retrieve the characteristic absorption spectrum of bilayer MoS_2, which is composed of two significant optical resonances in the energy range between 1.8 and 2.1 eV. These two absorption peaks have been assigned to the neutral A exciton transition at 1.95 eV, as well as the hybrid excitonic state which mixes A-interlayer and B-intralayer states [see Fig. 1(c)] (denoted as X^H in the following). We point out that this hybrid mode displays a significant reflection signal, caused by a strong oscillator strength that is only smaller by approximately a factor of 4 as compared to the intralayer A exciton.

Evident from the bias-dependent reflectivity measurements in Fig. 2(a), the applied static electric field couples to out of plane dipoles via the Stark effect, modifying the exciton energy as $\Delta E_X = \mathbf{d} \cdot \mathbf{E}$, with $\mathbf{d}$ the out of plane electric dipole and $\mathbf{E}$ the electric field. Since the X^H dipole is not polarized in our white light reflection experiment, both dipole (pointing from layer 1 to layer 2 and vice versa) coexist at the same energy at zero electric field. The out of plane electrical field lifts this degeneracy ending up with two different absorption lines in the spectrum [Fig. 2(a)]. We note that the application of only 5 V to our device yields a giant dipolar splitting of 100 meV of the two modes, which is only accompanied by a modest quenching of the oscillator strength.

Importantly, as we increase our gate voltage, we do not observe any signatures of the emergence of an attractive polaron in the reflectivity response of our device [20], which signifies that we remain in a low doping regime

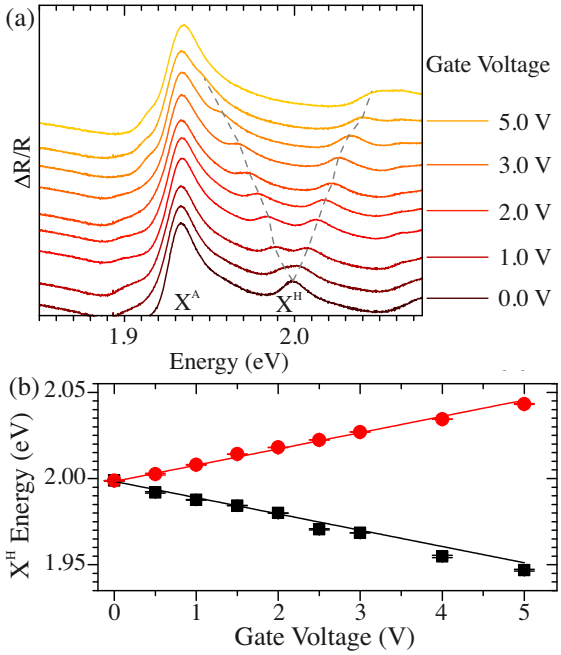

FIG. 2. (a) Cascade plot of the sample differential reflectivity at various gate voltage. (b) X^H energy with respect to the gate voltage for both dipole orientations (black squares and red dot). The red and black lines are linear fits to the data to extract the dipole size.

throughout our experiment, and the accumulation of supplementary charges via the gating process only will have a marginal impact of the observed physics.

For a quantitative analysis, we estimate the electric field from the gate voltage and the device geometry via a plate capacitor model ($\varepsilon_{\mathrm{BN}} = 3.76$, $\varepsilon_{\mathrm{MoS2}} = 6.8$ [21]), following the approach discussed in Ref. [22] (see Supplemental Material [23], notes). We extracte the emission energy of both X^H upper and lower branch which scales linearly with the gate voltage. By fitting our data, we directly yield a giant dipole moment of 0.48 ± 0.1 nm (uncertainties are based on s.d. values based on a least square fit to the data) for X^H, which is approximately a factor of 2 smaller than the interlayer distance of 1 nm [Fig. 2(b)], and matches the phenomenological expectation of a layer-localized electron coupling to a hole that is delocalized over both layers.

To further analyze the character of the hybrid excitonic mode, we study its behavior in an externally applied magnetic field. Therefore, we excited our bilayer nonresonantly with a linearly polarized 532 nm cw laser with a power of 2.5 mW at the entrance window of our cryostat focused onto a 3 μm diameter spot. We recorded the emitted photoluminescence (PL) for varying gate voltage and applied magnetic fields. We furthermore applied polarization resolved spectroscopy to extract the characteristic Zeeman splitting that is reflected by the energetic difference of the circular left and right polarized emission.

Figure 3(a) depicts the evolution of the photoluminescence as a function of the applied gate voltage at 0 T.

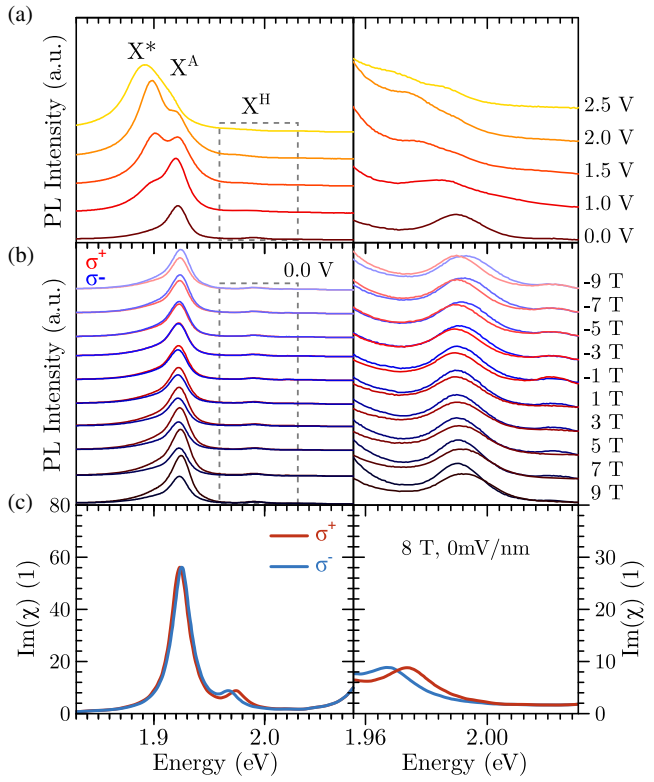

FIG. 3. (a) Left panel, PL spectra at different gate voltage at 0 magnetic field. The lowest lying emission line corresponds to the trion emission and is denoted X^*, the neutral intralayer exciton is denoted X^A and the hybrid exciton is denoted X^H. Right panel, close up around X^H (b) PL spectra at 0 gate voltage at different magnetic field. Right panel is a close up around X^H. (c) Simulated polarization resolved dielectric susceptibility at a magnetic field of $B_z = 8$ T.

Because of the lower energy of the X^A transition, most of the luminescence stems from this mode. The PL from X^H is quenched by approximately a factor of 10, but remains visible in the spectra (see right, zoomed panel). Evidently, when the bias voltage is raised up to 2.5 V, a third, redshifted peak appears and eventually dominates the luminescence response the spectrum, which we assign to the charged intralayer excitonic state of the bilayer.

Importantly, as depicted in Fig. 3(b), a notable polarization splitting in both the X^A transition as well as the X^H transition occurs in the presence of an applied magnetic field. A closer inspection indeed reveals that this magnetic field splitting of the two modes displays an opposite sign, and a substantially modified magnitude: at -9 T, the X^A mode experiences a splitting of 0.8 meV, whereas the X^H mode splitting exceeds -2 meV. To further quantify this behavior, we analyzed the extracted peak positions as a function of the applied magnetic field, yielding the g factor of the X^A exciton as -2. This, indeed, contrasts the commonly observed g factors fluctuating around -4 for A excitons in TMDC monolayers, but we note that, in particular, in MoS_2 monolayers g factors of -2 have been reported [31,32]. In our experiment, the g factor of the hybrid X^H, however, acquires a value of approximately 4.2. This already suggests that X^A and X^H are of fundamentally different character, and admix different valley contributions. To investigate the Zeeman and Stark shifts of intralayer and interlayer states, we carry out a microscopic analysis in the Heisenberg equation of motion framework with a Hamiltonian parametrized from DFT calculations [18,33]. The Coulomb potential, relevant for the binding of intralayer and interlayer excitons, is obtained from a static solution of the Poisson equation [34,35]. The radiative coupling of intralayer excitons is taken into account via solving Maxwell equations in a planar geometry [36]. The Stark shifts of the electronic bands in both monolayers are obtained from DFT calculation [18]. Last we take account of the Zeeman shifts of the bands [37], which include the effect of spin magnetic moment [3,38], orbital magnetic moment [4,6], and valley magnetic moment [39,40]. A detailed description of the theoretical approach can be found in the Supplemental Material [23], Sec. II.

To understand the different g factors of intralayer and interlayer exciton, we perform the following analysis: the g factor of an excitonic transition is given as the difference of conduction and valence band contributions $g = g^c - g^v$. For the intralayer exciton, we have $g_{\text{intra}} = g^c_{\text{valley}} - (g^v_{\text{orbital}} + g^v_{\text{valley}})$. The valley contributions of conduction and valence band compensate each other and the total g factor g_{intra} is dominated by the orbital contribution of the valence band. In contrast, for the interlayer transition, the hole is located in the other layer and has therefore opposite Zeeman shifts. For the resulting g factor $g_{\text{inter}} = g^c_{\text{valley}} - (-g^v_{\text{valley}} - g^v_{\text{orbital}})$ we find an addition of the valley contributions and the orbital contribution of the valence band in the other layer.

Next, we calculate the excitonic binding energies and wave functions for intra- and interlayer excitons by exploiting the Wannier equation and access the linear optical response via calculating the equation of motion for the exciton, as detailed in the Supplemental Material [23]. Our calculations yield binding energies of 163 meV for intralayer and an encouragingly large binding energy of 112 meV for the interlayer A excitons. This large excitonic binding energy is consistent with the recent observation of room-temperature absorption from the interlayer A exciton by Gerber *et al.* [19].

Figure 3(c) illustrates the imaginary part of the dielectric susceptibility of the bilayer. Without the inclusion of the tunneling in the equation of motion [Supplemental Material [23], Eq. (8)] only the A and B transitions occur in the spectrum (see Supplemental Material [23]). Inclusion of the tunneling yields a weak resonance above the A exciton, being associated with the interlayer A exciton, forming an optically allowed transition through hybridization of intralayer B and interlayer A excitons.

Applying a magnetic field to our model in Fig. 3(c) illustrates the polarization resolved dielectric susceptibility. Here, we consider a magnetic field of 8 T. We observe a splitting of all resonances, in particular, the intralayer transitions exhibit a negative g factor whereas the interlayer transition exhibits a positive one of much larger magnitude and opposite sign, clearly reproducing the phenomenological behavior captured in our experiment. A detailed analysis shows that for the intralayer exciton, the valley contributions to the Zeeman shift for electron and hole almost cancel, and the total Zeeman shift is dictated by the orbital contribution. In contrast, for the interlayer transition, while electron and hole stem from different layers, the valley contribution is adding up. Additionally, while the hole is located in the other layer compared to the intralayer A transition, the orbital contribution has opposite sign, which adds up with the valley contribution.

The hybridization of energy bands, giving rise to the X^H exciton resonance can be expected to sensibly react on the precise mode energy [the detuning between the indicated transitions sketched in Fig. 1(c)], and thus can be manipulated by the externally applied electric field. We check this hypothesis by repeating to determine the Zeeman splittings for the captured many-particle complexes for a variety of applied gate voltages Figs. 4(a)–4(d) and plot the extracted Zeeman splittings as a function of the gate voltage: The trion emission indeed only displays a modest modification

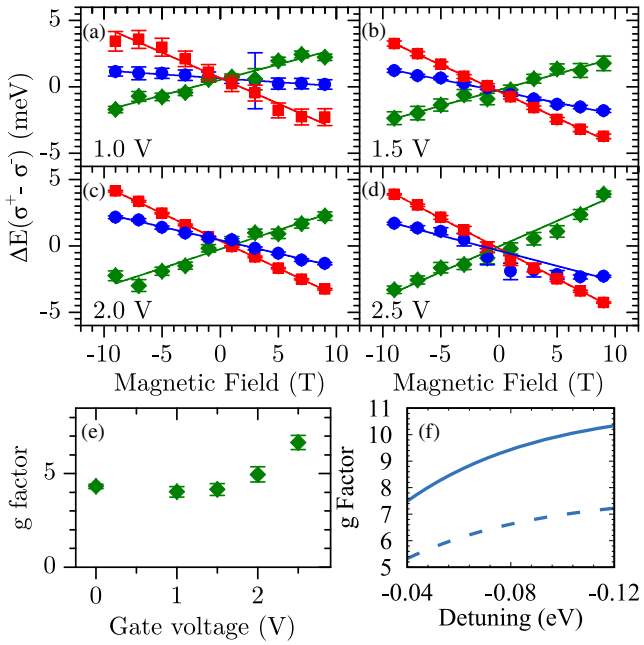

FIG. 4. (a)–(d) Zeeman splittings extracted at various bias conditions (1–2 V) for X^* (red square), X^A (blue dot), and X^H green diamond. (e) g factor for X^H with respect to the gate voltage. (f) Model curve for the g factor for X^H with respect to the gate voltage, based on the phenomenological approach introduced in Eq. (9). The two different curves utilize different g factors for the MoS_2 B exciton as well as the interlayer exciton.

of the extracted g factor, and the g factor of the exciton X^A fluctuates around a value of -2. More importantly, the hybrid exciton X^H, which stands in the focus of this study, displays a progressive increase of the g factor from 4.2 at 0 up to 7 at 2.5 V [Fig. 4(e)].

The reason for this behavior is the combined action of tunnel coupling of the interlayer excitons to the B exciton (which leads to a mixing of the g factors) and the tuning of the energetic position of the interlayer exciton. Without coupling, let us assume first that a pure interlayer exciton would have a g factor of about 12 and the B exciton of about -3. We note, however, that in particular in the MoS_2 system, strongly fluctuating g factors are observed throughout the literature (those typically scatter between -2 and -4.5 for the A exciton) [31,32], hinting at an utmost sensible dependence on the precise band structure, which is sensibly reacting on the surrounding. Now, coupling between the B exciton and the interlayer exciton leads to redistribution of the g factors among them, which becomes efficient if the interlayer exciton and the B exciton are weakly detuned. The applied electric field increases the detuning for the studied lower interlayer exciton from the B exciton resulting in an increasing g factor.

This can be phenomenologically captured in a simplified model including only the B exciton P^B and one interlayer exciton P^I. The simplified Bloch equations read [41]

$$(\hbar\omega - \tilde{E}^B)P^B = \Omega + TP^I, \tag{1}$$

$$(\hbar\omega - \tilde{E}^I)P^I = TP^B, \tag{2}$$

with the energies $\tilde{E}^B = E^B + g_B B_z$ and $\tilde{E}^I = E^I + g_I B_z$ and $E^I = E^B + \Delta$, $\Delta < 0$. The new energies of these coupled oscillator equations are given as

$$(\hbar\omega)_\pm = \frac{\tilde{E}^B + \tilde{E}^I}{2} \pm \sqrt{\frac{(\tilde{E}^B - \tilde{E}^I)^2}{4} + T^2} \tag{3}$$

$$= E_B + \frac{\Delta}{2} + \frac{g_B + g_I}{2} B_z \pm \sqrt{\frac{[(g_B - g_I)B_z - \Delta)^2]}{4} + T^2}, \tag{4}$$

where the $+$ solution refers to the B transition and the lower solution refers to the interlayer transition. The effective g^{eff} factor is given as

$$g_\pm^{\text{eff}} = (\partial_{B_z}(\hbar\omega)_\pm|_{B_z=0} = \frac{g_B + g_I}{2} \mp \frac{(g_B - g_I)\Delta}{4\sqrt{T^2 + \frac{\Delta^2}{4}}}. \tag{5}$$

We can now plot the effective g factor as a function of the detuning Δ in Fig. 4(f). We notice, despite a slight offset, the model captures the observed phenomenological behavior of the bias-tunable g factor of X^H. Indeed, the

quantitative deviation most likely arises from uncertainties associated with the g factor of the (uncoupled) interlayer transition and the B exciton, which are not experimentally accessible in our study. However, we notice that our A-interlayer exciton indeed displays g factor of ≈ -2, rather than the canonical value of -4 captured for most other TMDC A-exciton complexes. Let us thus consider reduced g factors of the B exciton as well as the interlayer exciton, rescaled by a factor of 1.5. Note, that the monotonous behavior of Eq. (9) does not depend on the precise choice of the interlayer excitons g factor, as long as it is larger than -2. We note that the dashed line depicted in Fig. 4(f) manages to quantitatively capture the experimentally observed tuning range of the interlayer exciton and the interlayer exciton g factor.

In conclusion, we have demonstrated the existence of an interlayer exciton in pristine bilayer MoS_2, which is characterized by a giant dipole moment in conjunction with a persistent oscillator strength. We have analyzed the behavior of this new excitonic species in an applied external electric and magnetic field, and found evidence for the mixing of K and K' valley states, contributing to the exciton. The valley character is tunable in an externally applied electric field, by modifying the effective interlayer vs intralayer character. Dipolar excitons with strong oscillator strength are of paramount importance for microcavity experiments in the regime of strong light-matter coupling. We anticipate that the interlayer exciton in pristine bilayer MoS_2 can be utilized to generate strongly interacting, dipolar exciton polaritons based on atomically thin materials.

Methods.—Sample fabrication: MoS_2 sheets were isolated from home-made flux zone grown MoS_2 crystals. The process started with 6N purity metal powder (Mo) and sulfur ingot pieces. Additional care was given to performing in-house purification to eliminate all the other contamination (typically heavy metals and magnetic metals) to reach true 6N purity. Crystal growth was performed using flux zone growth technique without any transporting agents to capture high quality crystals. The bilayers were then isolated using the dry transfer technique introduced in Castellanos-Gomez *et al.* [42]. We exfoliate our 2D materials on a transparent PolyDimethylSiloxane (PDMS) film. From this film, we transfer the 2D layers on a Si/SiO_2 substrate (with 100 nm SiO_2) with prepatterned gold contact, that were initially deposited on the substrate via e-beam assisted evaporation. The electrode are composed of a 3 nm thick Cr layer covered by 50 nm thick gold layer. The contact are prepatterned on the Si/SiO_2 substrate and the heterostructure is stacked on top of them directly.

The Würzburg group gratefully acknowledges support by the state of Bavaria. C. S. acknowledges funding with the ERC project unLiMIt-2D (Project No. 679288) and the Deutsche Forschungsgemeinschaft (DFG, German Research Foundation) with the priority programm SPP 2244 (DFG SCHN1376 14.1). This work was funded by the Deutsche Forschungsgemeinschaft (DFG, German Research Foundation)–INST 93/932-1 FUGG. Technical support by M. Emmerling and A. Wolf is acknowledged. S. T acknowledges support from DOE-SC0020653, NSF CMMI 1933214, NSF DMR 1552220 and DMR 1955889. We acknowledge fruitful discussions with our colleague Dominik Christiansen (TU Berlin), and support by Dr. C. Anton-Solanas and O. Iff for assistance in the graphics. The TUB group was funded by the Deutsche Forschungsgemeinschaft via projects 182087777 in SFB 951 (project B12, M. S. and A. K.) and KN 427/11-1 (F. K. and A. K.). F. K. thanks the Berlin School of Optical Sciences and Quantum Technology.

Note added.—Recently, we became aware of a an independent, similar work [43].

[1] G. Wang, A. Chernikov, M. M. Glazov, T. F. Heinz, X. Marie, T. Amand, and B. Urbaszek, Colloquium: Excitons in atomically thin transition metal dichalcogenides, Rev. Mod. Phys. **90**, 021001 (2018).

[2] J. R. Schaibley, H. Yu, G. Clark, P. Rivera, J. S. Ross, K. L. Seyler, W. Yao, and X. Xu, Valleytronics in 2d materials, Nat. Rev. Mater. **1**, 16055 (2016).

[3] Z. Gong, G.-B. Liu, H. Yu, D. Xiao, X. Cui, X. Xu, and W. Yao, Magnetoelectric effects and valley-controlled spin quantum gates in transition metal dichalcogenide bilayers, Nat. Commun. **4**, 2053 (2013).

[4] A. Srivastava, M. Sidler, A. V. Allain, D. S. Lembke, A. Kis, and A. Imamoğlu, Valley zeeman effect in elementary optical excitations of monolayer WSe_2, Nat. Phys. **11**, 141 (2015).

[5] A. V. Stier, K. M. McCreary, B. T. Jonker, J. Kono, and S. A. Crooker, Exciton diamagnetic shifts and valley zeeman effects in monolayer ws 2 and mos 2 to 65 tesla, Nat. Commun. **7**, 10643 (2016).

[6] G. Aivazian, Z. Gong, A. M. Jones, R.-L. Chu, J. Yan, D. G. Mandrus, C. Zhang, D. Cobden, W. Yao, and X. Xu, Magnetic control of valley pseudospin in monolayer WSe_2, Nat. Phys. **11**, 148 (2015).

[7] C. Robert, B. Han, P. Kapuscinski, A. Delhomme, C. Faugeras, T. Amand, M. R. Molas, M. Bartos, K. Watanabe, T. Taniguchi *et al.*, Measurement of the Spin-Forbidden Dark Excitons in MoS_2 and $MoSe_2$ monolayers, Nat. Commun. **11**, 4037 (2020).

[8] A. Chernikov, T. C. Berkelbach, H. M. Hill, A. Rigosi, Y. Li, O. Burak Aslan, D. R. Reichman, M. S. Hybertsen, and T. F. Heinz, Exciton Binding Energy and Nonhydrogenic Rydberg Series in Monolayer WS_2, Phys. Rev. Lett. **113**, 076802 (2014).

[9] F. Katsch, M. Selig, and A. Knorr, Exciton-Scattering-Induced Dephasing in Two-Dimensional Semiconductors, Phys. Rev. Lett. **124**, 257402 (2020).

[10] Q. H. Wang, K. Kalantar-Zadeh, A. Kis, J. N. Coleman, and M. S. Strano, Electronics and optoelectronics of

two-dimensional transition metal dichalcogenides, Nat. Nanotechnol. **7**, 699 (2012).
[11] N. Lundt, S. Klembt, E. Cherotchenko, S. Betzold, O. Iff, A. V. Nalitov, M. Klaas, C. P. Dietrich, A. V. Kavokin, S. Höfling *et al.*, Room-temperature tamm-plasmon exciton-polaritons with a WSe_2 monolayer, Nat. Commun. **7**, 13328 (2016).
[12] X. Liu, T. Galfsky, Z. Sun, F. Xia, E.-c. Lin, Y.-H. Lee, S. Kéna-Cohen, and V. M. Menon, Strong light–matter coupling in two-dimensional atomic crystals, Nat. Photonics **9**, 30 (2015).
[13] C. Schneider, M. M. Glazov, T. Korn, S. Höfling, and B. Urbaszek, Two-dimensional semiconductors in the regime of strong light-matter coupling, Nat. Commun. **9**, 2695 (2018).
[14] P. Rivera, J. R. Schaibley, A. M. Jones, J. S. Ross, S. Wu, G. Aivazian, P. Klement, K. Seyler, G. Clark, N. J. Ghimire *et al.*, Observation of long-lived interlayer excitons in monolayer mose 2–WSe_2 heterostructures, Nat. Commun. **6**, 6242 (2015).
[15] J. Horng, T. Stroucken, L. Zhang, E. Y. Paik, H. Deng, and S. W. Koch, Observation of interlayer excitons in $MoSe_2$ single crystals, Phys. Rev. B **97**, 241404(R) (2018).
[16] I. Niehues, A. Blob, T. Stiehm, S. M. de Vasconcellos, and R. Bratschitsch, Interlayer excitons in bilayer MoS_2 under uniaxial tensile strain, Nanoscale **11**, 12788 (2019).
[17] A. Arora, M. Drüppel, R. Schmidt, T. Deilmann, R. Schneider, M. R. Molas, P. Marauhn, S. M. de Vasconcellos, M. Potemski, M. Rohlfing *et al.*, Interlayer excitons in a bulk van der Waals semiconductor, Nat. Commun. **8**, 639 (2017).
[18] T. Deilmann and K. S. Thygesen, Interlayer excitons with large optical amplitudes in layered van der waals materials, Nano Lett. **18**, 2984 (2018).
[19] I. C. Gerber, E. Courtade, S. Shree, C. Robert, T. Taniguchi, K. Watanabe, A. Balocchi, P. Renucci, D. Lagarde, X. Marie, and B.Urbaszek, Interlayer excitons in bilayer MoS_2 with strong oscillator strength up to room temperature, Phys. Rev. B **99**, 035443 (2019).
[20] M. Sidler, P. Back, O. Cotlet, A. Srivastava, T. Fink, M. Kroner, E. Demler, and A. Imamoglu, Fermi polaron-polaritons in charge-tunable atomically thin semiconductors, Nat. Phys. **13**, 255 (2017).
[21] A. Laturia, M. L. Van de Put, and W. G. Vandenberghe, Dielectric properties of hexagonal boron nitride and transition metal dichalcogenides: from monolayer to bulk, npj 2D Mater. Appl. **2**, 6 (2018).
[22] Z. Wang, Y. H. Chiu, K. Honz, K. F. Mak, and J. Shan, Electrical tuning of interlayer exciton gases in WSe_2 bilayers, Nano Lett. **18**, 137 (2018).
[23] See Supplemental Material at http://link.aps.org/supplemental/10.1103/PhysRevLett.126.037401 additional details on sample characterization, theoretical and computational methodology. Refs. [24–30] are part of the Supplemental Section.
[24] A. Kormányos, V. Zólyomi, N. D. Drummond, and G. Burkard, Spin-oorbit Coupling, Quantum Dots, and Qubits in Monolayer Transition Metal Dichalcogenides, Phys. Rev. X **4**, 011034 (2014).
[25] Z. Lu, D. Rhodes, Z. Li, D. Van Tuan, Y. Jiang, J. Ludwig, Z. Jiang, Z. Lian, S. Shi, J. C. Hone, H. Dery, and D. Smirnov, Magnetic field mixing and splitting of bright and dark excitons in monolayer $MoSe_2$, 2D Mater. **7**, 015017 2019.
[26] Z. Y. Zhu, Y. C. Cheng, and U. Schwingenschlögl, Giant spin-orbit-induced spin splitting in two-dimensional transition-metal dichalcogenide semiconductors, Phys. Rev. B **84**, 153402 (2011).
[27] D. Xiao, G.-B. Liu, W. Feng, X. Xu, and W. Yao, Coupled Spin and Valley Physics in Monolayers of MoS_2 and other Group-VI Dichalcogenides, Phys. Rev. Lett. **108**, 196802 (2012).
[28] T. Cao, G. Wang, W. Han, H. Ye, C. Zhu, J. Shi, Q. Niu, P. Tan, E. Wang, B. Liu, and J. Feng, Valley-selective circular dichroism of monolayer molybdenum disulphide, Nat. Commun. **3**, 887 (2012).
[29] K. Kośmider, J. W. González, and J. Fernández-Rossier, Large spin splitting in the conduction band of transition metal dichalcogenide monolayers, Phys. Rev. B **88**, 245436 (2013).
[30] A. Kuc and T. Heine, The electronic structure calculations of two-dimensional transition-metal dichalcogenides in the presence of external electric and magnetic fields, Chem. Soc. Rev. **44**, 2603 (2015).
[31] M. Goryca, J. Li, A. V. Stier, T. Taniguchi, K. Watanabe, E. Courtade, S. Shree, C. Robert, B. Urbaszek, X. Marie *et al.*, Revealing exciton masses and dielectric properties of monolayer semiconductors with high magnetic fields, Nat. Commun. **10**, 4172 (2019).
[32] F. Cadiz, E. Courtade, C. Robert, G. Wang, Y. Shen, H. Cai, T. Taniguchi, K. Watanabe, H. Carrere, D. Lagarde *et al.*, Excitonic Linewidth Approaching the Homogeneous Limit in MoS_2-Based van der Waals Heterostructures, Phys. Rev. X **7**, 021026 (2017).
[33] A. Kormanyos, G. Burkard, M. Gmitra, J. Fabian, V. Zolyomi, N. D. Drummond, and V. Falko, k p theory for two-dimensional transition metal dichalcogenide semiconductors, 2D Mater. **2**, 022001 (2015).
[34] S. Ovesen, S. Brem, C. Linderälv, M. Kuisma, T. Korn, P. Erhart, M. Selig, and E. Malic, Interlayer exciton dynamics in van der waals heterostructures, Commun. Phys. **2**, 23 (2019).
[35] S. Brem, J. Zipfel, M. Selig, A. Raja, L. Waldecker, J. D. Ziegler, T. Taniguchi, K. Watanabe, A. Chernikov, and E. Malic, Intrinsic lifetime of higher excitonic states in tungsten diselenide monolayers, Nanoscale **11**, 12381 (2019).
[36] T. Stroucken, A. Knorr, P. Thomas, and S. W. Koch, Coherent dynamics of radiatively coupled quantum-well excitons, Phys. Rev. B **53**, 2026 (1996).
[37] D. MacNeill, C. Heikes, K. Fai Mak, Z. Anderson, A. Kormányos, V. Zólyomi, J. Park, and D. C. Ralph, Breaking of Valley Degeneracy by Magnetic Field in Monolayer $MoSe_2$, Phys. Rev. Lett. **114**, 037401 (2015).
[38] M. Van der Donck, M. Zarenia, and F. M. Peeters, Strong valley Zeeman effect of dark excitons in monolayer transition metal dichalcogenides in a tilted magnetic field, Phys. Rev. B **97**, 081109(R) (2018).
[39] W. Yao, D. Xiao, and Q. Niu, Valley-dependent optoelectronics from inversion symmetry breaking, Phys. Rev. B **77**, 235406 (2008).

[40] X. Xu, W. Yao, D. Xiao, and T. F. Heinz, Spin and pseudospins in layered transition metal dichalcogenides, Nat. Phys. **10**, 343 (2014).

[41] F. Katsch, M. Selig, and A. Knorr, Theory of coherent pump–probe spectroscopy in monolayer transition metal dichalcogenides, 2D Mater. **7**, 015021 (2019).

[42] A. Castellanos-Gomez, M. Buscema, R. Molenaar, V. Singh, L. Janssen, H. S. J. Van Der Zant, and G. A. Steele, Deterministic transfer of two-dimensional materials by all-dry viscoelastic stamping, 2D Mater. **1**, 011002 (2014).

[43] N. Leisgang *et al.*, Giant Stark splitting of an exciton in bilayer MoS_2Nat. Nanotech. **15**, 901 (2020).